DINAME 2023 - Proceedings of the XIX International Symposium on Dynamic Problems of Mechanics,
A.S. De Paula, A.T. Fabro and M.R. Machado (Editors), ABCM.
Pirenópolis, Go, Brazil, February 26th to March 3rd, 2023

Wave and Modal Analysis of Band Gap Formation in Periodic Rotors

P. B. Lamas[1] **and R. Nicoletti**[1]

[1] University of São Paulo, São Carlos School of Engineering, São Carlos-SP, 13566-590, Brazil

Abstract: In this work we study the band gap formation in periodic rotors through modal and wave analysis. It is shown that band gaps are zones where no resonances appears, with a low vibration response, large bandwidth and where there is no propagating waves. The gyroscopic effect in the band gap formation is evaluated through a Campbell diagram and it is shown that the rotating speed does not significantly affect the band gap formation.

Keywords: wave propagation, periodic structures, rotating systems, structural vibration, WFE

INTRODUCTION

Rotating machines are mainly composed by a rotating shaft with working elements (impellers) mounted on it. These working elements adds localized mass and inertia in the system and, when these inertia are evenly distributed along the shaft, a dynamic effect occurs: band gap zones in the frequency spectrum (Richards and Pines, 2003). These regions are characterized by the lack of resonances, low system's response to excitation, and bandwidth much bigger than the average distance between two resonances of the system (Deymier, 2003). These characteristics are interesting for rotating systems since they operate at specific frequency ranges. Thus, by placing the operating range of the machine in a band gap zone, we guarantee a low vibration response with a good safety margin.

Any periodic structure can present bandgaps in their frequency spectrum (Bachour and Nicoletti, 2020). In this study area, the WFE (Wave Finite Element) method is an approach to study the wave motion in periodic structures. Basically, the unit cell used to built the periodic structure (Fig. 1) is modelled using FEM (Finite Element Method). Then, the equations of motion are obtained in frequency domain and periodicity conditions are applied. This leads to an eigenvalue problem whose solutions are the dispersion curves and wavemodes.

In the present work, we analyze the band gap formation in periodic rotors. To do that, we use as the unit cell that compose the rotating periodic structure: a section of shaft with a single rigid disk in the middle (Fig. 1). Modal and Wave analysis are made to shown that the band gap regions are zones where no resonances appears, with a low vibration response, large bandwidth and where there is no propagating waves. Finally, the gyroscopic effect in the band gap formation is evaluated through a Campbell diagram, it is shown that the rotating speed does not significantly affect the band gap formation.

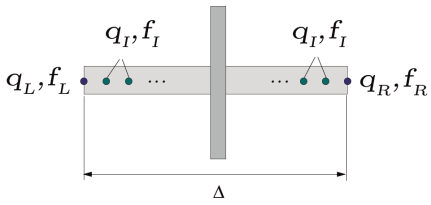

Figure 1 – Rotor unit cell used to built the periodic rotor.

MATHEMATICAL MODELING

Consider a rotor with working elements periodically mounted along with the shaft, as depicted in Fig. 2 using the unit cell shown in Fig. 1. The adopted mathematical model of the rotor is based on Finite Elements based on the Euler-Bernoulli theory, where the working elements (impellers) are considered rigid (Nelson and McVaugh, 1976). The same analysis can be made using finite elements based on the Timoshenko beam theory (Nelson and McVaugh, 1980). The shaft finite element has a constant radius and constant material properties, and it has two nodes, each one with four degrees-of-freedom: translation in lateral directions (x_i and y_i) and rotation around X and Y directions (β_i and d γ_i). By adopting a mesh of N connected elements to model the shaft, one arrives in a system of equations of the form:

$$\mathbf{M}_S\ddot{\mathbf{z}}_S + (\mathbf{D}_S - \Omega\mathbf{G}_S)\dot{\mathbf{z}}_S + \mathbf{K}_S\mathbf{z}_S = \mathbf{0} \tag{1}$$

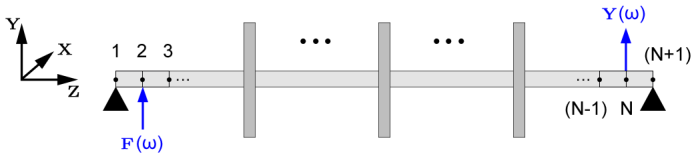

Figure 2 – Finite element representation of the rotor with the excitation ($\mathbf{F}(\omega)$) and response ($\mathbf{Y}(\omega)$) points used to calculate the FRF.

where $\mathbf{M}_S$, $\mathbf{D}_S$, $\mathbf{G}_S$ and $\mathbf{K}_S$ are the shaft inertia, the damping matrix, the gyroscopic matrix, and the stiffness matrix, respectively, Ω is the rotating speed of the rotor (in rad/s), and $\mathbf{z}_S$ is the vector of all degrees of freedom of the shaft:

$$\mathbf{z}_S = \{ \; x_1 \quad y_1 \quad \beta_1 \quad \gamma_1 \quad \cdots \quad x_i \quad y_i \quad \beta_i \quad \gamma_i \quad \cdots \quad x_{N+1} \quad y_{N+1} \quad \beta_{N+1} \quad \gamma_{N+1} \; \}^T \tag{2}$$

where N is the number of finite shaft elements in the model. The elements that represent the impellers are modeled as rigid disks. Hence, they are represented in the model by their masses and moments of inertia, which are added to the inertia matrix and to the gyroscopic matrix according to their position in the rotor, i.e. according to the node where the impeller is located in the model. The finite element matrices used in the model are found in (Nelson and McVaugh, 1976).

By adopting this model, one can find the natural frequencies of the rotor from the eigenvalues of the system in state-space formulation. The eigenvalues of the system are obtained by solving the eigenvalue problem below:

$$\begin{bmatrix} \mathbf{M}_s & \mathbf{0} \\ \mathbf{0} & \mathbf{M}_s \end{bmatrix} \begin{Bmatrix} \ddot{\mathbf{z}}_s \\ \dot{\mathbf{z}}_s \end{Bmatrix} + \begin{bmatrix} \mathbf{D}_s - \Omega\mathbf{G}_s & \mathbf{K}_s \\ -\mathbf{M}_s & \mathbf{0} \end{bmatrix} \begin{Bmatrix} \dot{\mathbf{z}}_s \\ \mathbf{z}_s \end{Bmatrix} = \begin{Bmatrix} \mathbf{0} \\ \mathbf{0} \end{Bmatrix} \;\Rightarrow\; (\mathrm{i}\lambda\mathbf{A} + \mathbf{B})\,\mathbf{u} = \mathbf{0} \tag{3}$$

where λ is the system's eigenvalue, $\mathbf{u}$ is the system's eigenvector, and $\mathbf{A}$ and $\mathbf{B}$ are state-space matrices;

The frequency response function (FRF) of the system is obtained by calculating the receptance matrix:

$$\mathbf{H}(\omega) = \frac{\mathbf{Y}(\omega)}{\mathbf{F}(\omega)} = \left(-\omega^2\mathbf{M}_S + \mathrm{i}\omega\,(\mathbf{D}_S - \Omega\mathbf{G}_S) + \mathbf{K}_S\right)^{-1} \tag{4}$$

where ω is the excitation frequency.

In this work, all the results are based on the response in vertical direction of the first unconstrained node next to the first bearing due to an excitation in vertical direction at the last unconstrained node next to the second bearing (opposite side of the shaft) – see Fig. 2. In all analyses, the bearing allows rotational motion only (lateral displacements are constrained), thus representing the configuration of simply-supported rotor. As a rule, we adopt 10 finite elements between two disks or between a disk and a bearing (a number of elements large enough to assure natural frequency convergence).

Wave Analysis For Null Rotating Speed

Consider a finite mesh generated with elements that are delimited by only two nodes, this nodes can have n_{dofs} degrees of freedom (dofs) per node. The equations of motion in frequency domain are given by:

$$[\mathbf{K}_s - \omega^2\mathbf{M}_s]\mathbf{q} = \mathbf{f} \tag{5}$$

where,

$$\mathbf{q} = \begin{bmatrix} \mathbf{q_L} & \mathbf{q_I} & \mathbf{q_R} \end{bmatrix}^T, \;\; \mathbf{f} = \begin{bmatrix} \mathbf{f_L} & \mathbf{f_I} & \mathbf{f_R} \end{bmatrix}^T \tag{6}$$

where $\mathbf{q_L}$, $\mathbf{q_R}$, $\mathbf{f_L}$ e $\mathbf{f_R}$ are vectors composed by the left (L) and right (R) degrees of freedom, of nodal displacements and forces, respectively; and $\mathbf{q_I}$, $\mathbf{f_I}$ are vectors composed by the internal degrees of freedom of nodal displacements and forces, respectively.

The periodicity condition is given by:

$$\mathbf{q_R} = \lambda\mathbf{I}_{n_{dofs}}\mathbf{q_L} \tag{7}$$

where λ is the Bloch wavenumber:

$$\lambda = e^{-ik\Delta} \tag{8}$$

So by applying the periodicity condition we can rewrite $\mathbf{q}$ as follows:

$$\mathbf{q} = \begin{bmatrix} \mathbf{q_L} \\ \mathbf{q_I} \\ \mathbf{q_R} \end{bmatrix} = \Lambda_R \begin{bmatrix} \mathbf{q_L} \\ \mathbf{q_I} \end{bmatrix} = \begin{bmatrix} \mathbf{I}_{n_{dofs}} & \mathbf{0}_{n_{dofs}\times n_{id}} \\ \mathbf{0}_{n_{id}\times n_{dofs}} & \mathbf{I}_{n_{id}} \\ \lambda\mathbf{I}_{n_{dofs}} & \mathbf{0}_{n_{dofs}\times n_{id}} \end{bmatrix} \begin{bmatrix} \mathbf{q_L} \\ \mathbf{q_I} \end{bmatrix} \tag{9}$$

onde n_{id} is the number of internal degrees of freedom of the mesh; n_i is the number of internal nodes of the mesh; and $n_{id} = n_i \cdot n_{dofs}$. Equilibrium at node L implies that:

$$\mathbf{f_L} + \lambda^{-1}\mathbf{f_R} = \mathbf{0} \tag{10}$$

Also, the nodal forces of the internal nodes are considered zero. That means:

$$\mathbf{f_I} = \mathbf{0} \;\Rightarrow\; \Lambda_L \mathbf{f} = \mathbf{0} \tag{11}$$

or

$$\begin{bmatrix} \mathbf{I}_{n_{dofs}} & \mathbf{0}_{n_{dofs}\times n_{id}} & \lambda^{-1}\mathbf{I}_{n_{dofs}} \\ \mathbf{0}_{n_{id}\times n_{dofs}} & \mathbf{I}_{n_{id}} & \mathbf{0}_{n_{id}\times n_{dofs}} \end{bmatrix} \begin{bmatrix} \mathbf{f_L} \\ \mathbf{f_I} \\ \mathbf{f_R} \end{bmatrix} = \mathbf{0} \tag{12}$$

Substituting Eq. (9) in Eq. (5) and pre-multiplying by Λ_L, gives:

$$\Lambda_L[\mathbf{K}_s - \omega^2\mathbf{M}_s]\Lambda_R \begin{bmatrix} \mathbf{q_L} \\ \mathbf{q_I} \end{bmatrix} = \Lambda_L \begin{bmatrix} \mathbf{f_L} \\ \mathbf{f_I} \\ \mathbf{f_R} \end{bmatrix} \tag{13}$$

$$\bar{\mathbf{D}}(\lambda, \omega) \begin{bmatrix} \mathbf{q_L} \\ \mathbf{q_I} \end{bmatrix} = \mathbf{0} \tag{14}$$

where,

$$\bar{\mathbf{D}} = \Lambda_L \mathbf{K}_s \Lambda_R - \omega^2 \Lambda_L \mathbf{M}_s \Lambda_R \tag{15}$$

$\bar{\mathbf{D}}$ is the dynamic stiffness of the mesh with node R projected onto node L.

BAND GAP FORMATION IN PERIODIC ROTORS

Consider a slender rotor, whose properties are listed in Table 1. If we mount on the shaft a series of disks, evenly displaced (using the unit cell shown in Fig.) along the shaft, the system presents the natural frequencies and FRFs shown in Fig. 3a. As the number of disks in the system increases, there appear three regions where no natural frequencies occur in the system (regions 1, 2, and 3 in Fig. 3a). These are the band gaps formed by periodicity of disks on the shaft, which refer to the rotating speed of 1,000 rpm. We adopted such a low rotating speed for an easier understanding of the phenomena involved, but we show later that gyroscopic effects at higher rotating speeds do not significantly alter the results. Figure 3b shown the dispersion diagrams as a function of the number of disks unit cell for null rotating speed. As the number of disks in the system increases, that means, the unit cell length decreases, there appear three regions where no propagating waves occur in the system (blank regions 1, 2, and 3 in Fig. 3b). Also, it can be noted that in all no propagation zones (blank zones) there is no natural frequencies (dots) of the corresponding finite structure.

Table 1 – Properties of the rotors in study.

Property	Value	Unit
Shaft length (L)	600	mm
Shaft diameter (D)	10	mm
Disk diameter (D_D)	60	mm
Disk thickness (E_D)	5	mm
Young modulus (E)	2.1×10^{11}	$\mathrm{N.m^{-2}}$
Material density (ρ)	7850	$\mathrm{kg.m^{-3}}$

EFFECT OF ROTATING SPEED

To investigate the influence of greater gyroscopic effects, a Campbell diagram is presented in Fig. 4. As one can see, the natural frequencies split into two frequencies, which are associated with two precession modes (forward and backward) caused by the gyroscopic effect. This effect is magnified with increasing rotating speeds. As a result of the gyroscopic effect, the bandgap tends to narrow as the rotating speed increases. In this case, the first bandgap narrows by 7.5% at the rotating speed of 6,000 rpm, whereas the second bandgap decreases by 2.6%. Although we have a narrowing in the band gaps, its use is not impaired. The band gaps are still large enough for a safe machine operation. A similar behavior is expected in rotors with a different number of disks.

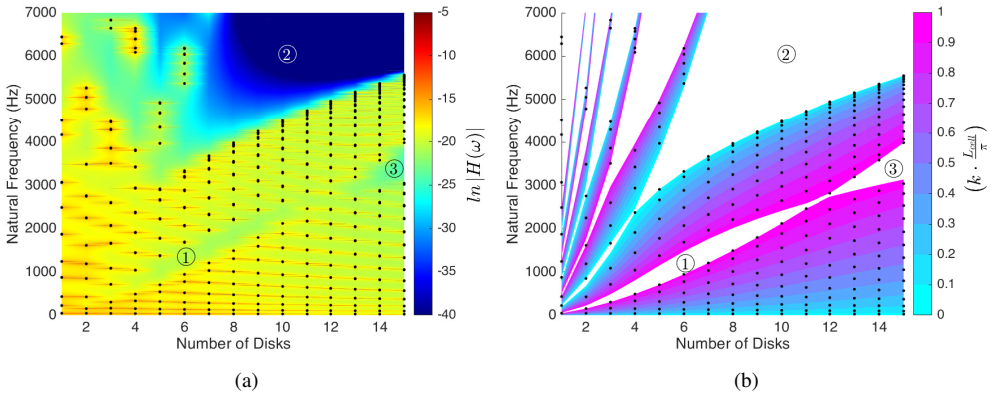

Figure 3 – Modal and Wave analysis of periodic rotors: (a) Natural frequencies (dots) and the amplitude of the FRF (colors) of the rotors as a function of the number of disks periodically distributed along the shaft (results for a rotating speed of 1000 rpm) and (b) Natural frequencies (dots) and normalized wavenumber (colors) as a function of the number of disks unit cell (results for a null rotating speed).

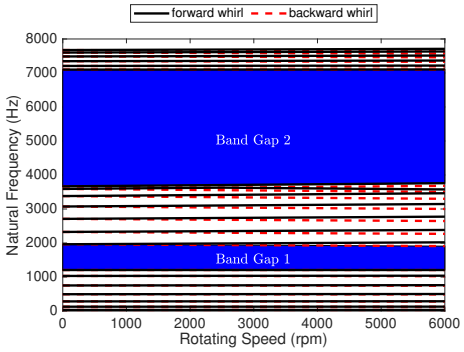

Figure 4 – Campbell diagram of the studied rotor with 7 disks.

CONCLUSIONS

The obtained results show that rotors with periodicity imposed by disks present band gaps in their frequency spectrum, i.e. zones with no resonance peaks, large bandwidth and low vibration response. Also, the dispersion diagrams show that these are regions where there is no propagating waves. The WFE method is a practical method, because once the matrices Λ_L and Λ_R are defined, we can easily obtain the dispersion and wavemodes any arbitrary structure modelled by FEM. Finally, the gyroscopic effect tends to narrow the gap bandwidth, but it is still large enough for a safe operation.

ACKNOWLEDGMENTS

This project was supported by the Brazilian research foundation CAPES, under grant no. 88887.484667/2020-00.

REFERENCES

Bachour, R.S. and Nicoletti, R., 2020, “Natural frequencies and band gaps of periodically corrugated beams”, Journal of Vibration and Acoustics, Vol. 143, No.4, doi:10.1115/1.4048889.

Deymier, P.A., 2013, “Acoustic Metamaterials and Phononic Crystals”, Springer Berlin Heidelberg, doi:10.1007/978-3-642-31232-8.

Nelson, H.D. and McVaugh, J. M., 1976, “The Dynamics of Rotor-Bearing Systems Using Finite Elements”, Journal of Engineering for Industry, Vol. 98, No. 2, pp.593-600, ISSN 0022-0817.

Nelson, H.D. and McVaugh, J. M., 1980, “Finite Rotating Shaft Element Using Timoshenko Beam Theory”, Journal of Mechanical Design, Vol. 102, No. 4, pp.793-803, ISSN 0161-8458, doi:10.1115/1.3254824.

Richards, D. and Pines, D., 2003 “Passive Reduction of Gear Mesh Vibration Using a Periodic Drive Shaft”, Journal of Sound and Vibration, Vol. 264, No. 2, pp. 317-342, doi:10.1016/s0022-460x(02)01213-0.

RESPONSIBILITY NOTICE

The author(s) is (are) the only responsible for the printed material included in this paper.